ORIGINAL PAPER

Electrochemical study of anatase TiO$_2$ nanotube array electrode in electrolyte based on 1,3-diethylimidazolium *bis*(trifluoromethylsulfonyl)imide ionic liquid

Milan Vraneš[1] · Nikola Cvjetićanin[2] · Snežana Papović[1] · Marko Pavlović[3] · István Szilágyi[4,5] · Slobodan Gadžurić[1]

Abstract

The density, viscosity and electrical conductivity of ionic liquid 1,3-diethylimidazolium *bis*(trifluoromethylsulfonyl)imide, (C$_2$C$_2$imTFSI), and 0.5-M solution of LiTFSI in C$_2$C$_2$imTFSI were determined at different temperatures. The LiTFSI/C$_2$C$_2$imTFSI system was tested as a possible electrolyte for lithium-ion batteries by using anatase TiO$_2$ nanotube array electrode as anode material for the first time. The electrochemical testing has shown not only the improvement of lithium-ion insertion/deinsertion properties by increasing temperature but also the existence of a decomposition of the electrolyte, detecting the change of colour. The decomposition of electrolyte leads to the formation of a film on the surface of the electrode which improves Coulombic efficiency during cycling.

Keywords Imidazolium ionic liquid · Ionicity · TiO$_2$ nanotubes · Cyclic voltammetry · Galvanostatic cycling

Introduction

Current lithium-ion battery (LIB) systems are not sufficiently safe mainly owing to undesired reactions between the battery components and flammable electrolytes [1, 2], triggered by unpredictable events such as short circuits or local overheating,

✉ Milan Vraneš
milan.vranes@dh.uns.ac.rs

1 Faculty of Science, Department of Chemistry, Biochemistry and Environmental Protection, University of Novi Sad, Trg Dositeja Obradovića 3, Novi Sad 21000, Serbia

2 Faculty of Physical Chemistry, University of Belgrade, Studentski trg 12-16, Belgrade 11158, Serbia

3 Department of Colloid Chemistry, Max-Planck Institute of Colloids and Interfaces, Am Mühlenberg 1, 14476 Potsdam, Germany

4 MTA-SZTE Lendület Biocolloids Research Group, University of Szeged, Szeged H-6720, Hungary

5 Interdisciplinary Excellence Center, Department of Physical Chemistry and Materials Science, University of Szeged, Szeged H-6720, Hungary

leading to an exothermic reaction of the electrolyte with the electrode materials [3, 4]. Electrolytes for LIBs derived from ionic liquids (ILs) exhibit negligible vapour pressure and flame-retardant performance [5] that ensure reliability in their use as safe electrolytes in LIBs and improve battery safety [6, 7], resulting with extreme temperature range operation. Novel battery architectures with improved safety, power and energy density are currently being demanded for battery miniaturization.

Indeed, the properties of ILs can be tailored in detail by the cation and anion combination. From a literature survey, it was observed that the most used and efficient anion was *bis*(-trifluoromethylsulfonyl)imide ([NTf$_2$]$^-$) due to the delocalized charge that it possesses, even if some drawbacks are reported to be related to its corrosive characters [8, 9]. Its advantages are high thermal stability and adapted physicochemical properties. As cations, imidazolium-based ones are often used to allow easy chemical modification by changing the length, the number and the functionality of the side-alkyl chains. Indeed, the presence of an acidic proton on the C2 position, which is reactive towards lithium, has to be considered [10–12]. Thus, many authors have attempted to improve the electrochemical stability by suitable modifications of the IL structure [7, 13–20]. However, the results are somewhat contradictory and some confusion still remains.

An electrode material which enhances the capacity and energy density of the battery could be TiO$_2$ nanotube arrays (NTAs) [21–32]. The most frequently mentioned potential

Springer

applications are the use of TiO$_2$ NTAs in photocatalysis and dye solar cells [33, 34]. Modification of the semiconductor nature of highly ordered TiO$_2$ NTAs is important for its application in constructing high-performance supercapacitors [35, 36]. Applications of TiO$_2$ NTAs in electrochromic devices, as improved photo-catalysts and anodes for micro LIBs, are connected with the modification of electronic and optical properties of TiO$_2$ upon lithium-ion (Li$^+$) intercalation and the ability of nanotubes to intercalate/deintercalate Li$^+$ large number of times [21–24].

As continuation of our scientific work [37, 38], in this research study are examined the physicochemical and electrochemical properties of 0.5 mol·dm^{-3} LiTFSI ionic liquid 1,3-diethylimidazolium bis(trifluoromethylsulfonyl)imide, C$_2$C$_2$imTFSI, as well as the performance of anatase Ti/TiO$_2$ nanotube array (NTA) cells—that electrode material enhances the capacity and energy density of the battery upon lithium-ion (Li$^+$) intercalation and the ability of nanotubes to intercalate/deintercalate Li$^+$ large number of times [39]. In order to examine temperature effect on cell performances, cyclic voltammetry (CV) and galvanostatic charge/discharge experiments are performed in a wide temperature range 298.15 to 328.15 K. The electrochemical testing was conducted in order to compare the stability of selected electrolyte with previous one, which contains γ-butyrolactone, GBL, as cosolvent [37], where it is assumed that there is a possibility of stabilization effect between the carbonyl group of GBL and acidic C2-H from 1,3-dialkylimidazolium cation. The aims of this work are to investigate electrochemical performances of electrolyte containing only lithium salt in ionic liquid and to realize a battery system that has both safety and high-energy performances.

Experimental

Materials

Ionic liquid C$_2$C$_2$imNTf$_2$ was commercially available from IoLiTec ($\omega \geq 0.99$). The summary of the provenance and purity of the samples is given in Table 1. The ionic liquid was slowly heated under vacuum for 1 day. Prior to use, the ionic liquid was kept in a vacuum desiccator over P$_2$O$_5$ for 24 h. After that, C$_2$C$_2$imNTf$_2$ was stored in a dry box under a nitrogen atmosphere. The water content in IL was determined by Karl Fischer titration using an 831 Karl Fischer coulometer, and the amount of water content is given in Table 1.

Lithium salt, LiTFSI, was dried in vacuum at $T = 373.15$ K. The electrolyte was prepared under inert conditions in an argon-filled glove box by dissolving LiTFSI in C$_2$C$_2$imTFSI, obtaining Li$^+$ concentration c(Li$^+$) = 0.5 mol·dm^{-3}. For convenience, in this work, the electrolyte 0.5 mol·dm^{-3} LiTFSI in C$_2$C$_2$imTFSI will be referred as LiTFSI/C$_2$C$_2$imTFSI.

TiO$_2$ NTAs were prepared by anodic oxidation of 0.25-mm thick and 0.5-cm wide Ti foil. The anodization was conducted in 0.7% glycerol solution of NH$_4$F by using graphite as a cathode, under a constant voltage of 30 V. The anodic oxidation was performed during 6 h to obtain a sufficiently thick layer of NTs [40] for accurate mass determination. Both sides of Ti electrode covered with NTs were well rinsed with distilled water, and after drying, the electrode was annealed three times in air at $T = 673.15$ K to convert TiO$_2$ from amorphous to crystal anatase form.

Apparatus and procedures

Density measurements

The vibrating tube Rudolph Research Analytical DDM 2911 densimeter with the accuracy and precision of $\pm$ 0.00005 g cm^{-3} was used for density measurements. The instrument was thermostated within $\pm$ 0.01 K and viscosity was automatically corrected. Before each series of measurements, calibration of the instrument was performed at the atmospheric pressure ($p = 0.1$ MPa) using ambient air and bi-distilled ultra-pure water in the temperature range from 293.15 to 323.15 K. Each experimental density value is the average of at least five measurements at selected temperatures. Repeated experimental measurements showed reproducibility within 0.01%, and an average value is presented in this paper. The standard uncertainty of determining the density is less than $7.6 \cdot 10^{-4}$ g cm^{-3}.

Viscosity measurements

The viscosity of pure ionic liquid was measured using a Brookfield Viscometer DV II+ Pro thermostated within $\pm$ 0.01 K and filled with about 8 cm^3 of liquid. The spindle type (SC4-18) was immersed and the rate per minute (RPM) was set to obtain a suitable torque. A viscometer cell was protected from moisture with the compartment made by the manufacturer and calibrated using the liquids of different viscosities purchased from the manufacturer. The viscosity of pure ionic liquid and electrolyte was measured in the temperature range from 293.15 to 323.15 K with a rotation speed of 60 RPM. Presented experimental values are the mean of three measurements and the measurement relative standard uncertainty was found to be about 1%.

Electrical conductivity measurements

These measurements were carried out in a Pyrex cell with platinum electrodes in the temperature range 293.15 to 323.15 K on a conductivity meter Jenco 3107, using a DC signal. The conductometric cell with a total volume of 14 cm^3 was initially dried in the atmosphere of nitrogen and

Table 1 Provenance and purity of the samples

Chemical name	Provenance	Product number	Purification method	Final mass fraction as stated by the supplier	Water analysis method	Water content (ppm)
C_2C_2imTFSI	IoLiTech	174,899–88-8	Vacuum drying	$\omega \geq 0.99$	KF titration	13
LiTFSI	Sigma-Aldrich	90,076–65-6	Vacuum drying	$\omega \geq 0.9995$	–	–
0.5 mol·dm^{-3} LiTFSI^c/C_2C_2imTFSI	–	–	Vacuum drying	–	KF titration	10
Ti foil	Alfa Aesar	7440-32-6	–	$\omega \geq 0.995$	–	–
NH$_4$F	Sigma-Aldrich	12,125–01-8	–	$\omega \geq 0.995$	–	–
Glycerol	Sigma-Aldrich	56–81-5	–	$\omega \geq 0.995$	–	–

C_2C_2imTFSI, 1,3-diethylimidazolium *bis*(trifluoromethylsulfonyl)imide

KF titration, Karl Fischer titration

LiTFSI, lithium *bis*(trifluoromethylsulfonyl)imide

thermostated for 20 min with the external flow with an accuracy of ± 0.01 K. At least 10 measurements were performed at 5 s intervals, in order to eliminate the self-heating and ionization in the electrodes [41]. The experimental cell was calibrated with standard 0.1000 mol dm^{-3} KCl solution by the same experimental procedure. The resulting cell constant amounted to 1.0353 cm^{-1}, and it was checked from time to time to control any possible evolution. The uncertainty for electrical conductivity was less than 1.5%. All obtained experimental values represent the mean of three measurements.

Flammability test

The potential flammability of the ionic liquid C_2C_2imTFSI and LiTFSI/C_2C_2imTFSI electrolyte could be examined by directly observing the flame on the surface of the solution for 60 s. Firstly, the ionic liquid or electrolyte sample (exactly measured mass) was placed to a watch glass and exposed to a burner for 60 s to allow ignition, but the flame from investigated samples was not observed. The flame temperature was 1200 °C, measured with a Digital Thermocouple Thermometer Dual-channel LCD Backlight Temperature Meter with an R-type Thermocouple sensor probe.

Electrochemical tests

The cyclic voltammetry (CV) experiments were carried by Gamry PCI4/300 Potentiostat/Galvanostat in a bottle-like three-electrode cell made of Pyrex glass and closed with a Teflon stopper with a double "O" ring. Electrical contacts for all three electrodes were routed through the Teflon stopper. The cell is filled with 3 cm^3 of the electrolyte. Ti foil with anodically grown TiO$_2$ NTAs was used as the working electrode, and lithium metal foil was used both as the reference and counter electrode. The geometrical surface area of the working electrode in contact with electrolyte was 1 cm^2. All CVs were recorded by using a current interrupt (CI) method for IR compensation. The same type of cell in a two-electrode arrangement was used for galvanostatic charging/discharging experiments which were performed by an Arbin BT 2042 battery testing device. The temperature control was achieved by immersing cells in the thermostat bath (Lauda UB 40J, WK 1400).

The same two-electrode cell used for galvanostatic experiments was also used for electrochemical impedance spectroscopy (EIS) measurements using a Gamry PCI4/300 Potentiostat/Galvanostat. The EIS measurements were performed at $T = 298.15$ K after 50 and 150 galvanostatic cycles. The cell was fully discharged and halfway charged at a current rate 20 μA·cm^{-2} and then left to relax half an hour before measurements. An AC amplitude of 5 mV was applied in the frequency range 100 kHz–0.1 (0.01) Hz. The Gamry Echem Analyst, version 5.61, was used for fitting data to the equivalent circuit model.

Raman, FTIR and UV-Vis spectroscopy measurements

Room temperature Raman spectra of electrolytes were obtained using solid-state Nd:YAG laser excitation line of 532 nm, with an incident laser power less than 60 mW on a Thermo Scientific DXR Raman microscope, under the inert atmosphere. A Tri Vista 557 triple spectrometer coupled with the nitrogen-cooled CCD detector was employed for spectrum collection.

The FTIR measurements were performed using a Thermo Scientific Nicolet iS20 spectrometer equipped with a

Universal diamond ATR Sampling Accessory. The measurements were performed with a total of 60 scans at room temperature and a spectrum resolution of 2 cm^{-1} in a range from 500 to 3400 cm^{-1}. Investigated electrolytes were placed on the top of the diamond crystal, and measurements were performed under the inert atmosphere. The Omnic 6.2 software was used for the data acquisition and spectral analysis.

In the wavelength range 250–800 nm, the absorption spectra were recorded. The measurements were performed on a Thermo Scientific UV-Vis spectrophotometer Evolution 220. Quartz spectrophotometric cells of 1-mm path length with Teflon stoppers were used, and all measurements were performed at room temperature and under the inert atmosphere.

Electrode material characterization, XRD and SEM

The crystal structure of TiO$_2$ NTAs was examined by X-ray diffraction (XRD). XRD data were collected by a Philips PW diffractometer 1050 with Cu-Kα1,2 radiation in a 2θ range between 20 and 80° with a step size 0.05° and counting time 2 s per step. XRD patterns of Ti foil, before and after anodization, are shown in Fig. S1. The reflections of both anatase and Ti-metal phase can be observed in the XRD pattern of Ti foil after anodic oxidation. The strongest and the most obvious reflections of the anatase phase are marked with an asterisk. A similar procedure for TiO$_2$ NTA preparation from Ti foil was demonstrated by Papović et al. [37].

The surface morphology of obtained TiO$_2$ NTs was investigated through a JEOL JSM 6460LV scanning electron microscope (SEM) (Fig. S2). The NTs have a more or less cylindrical shape with outer diameter of ~150 nm, inner diameter of ~80 nm and wall thickness of 35–40 nm. Obtained SEM images of TiO$_2$ NTAs before and after cycling did not show any change in morphology and structure (Fig. S3).

Results and discussion

Physicochemical properties for IL and IL-based electrolyte

Due to a lack of literature data for density, viscosity and electrical conductivity of C$_2$C$_2$imTFSI, these physicochemical properties were measured in the temperature range from 293.15 to 323.15 K and at an atmospheric pressure ($p =$ 0.1 MPa). The experimental results for C$_2$C$_2$imTFSI are presented in Table 2 and compared with some available experimental data from the literature [41–46].

It was found that density values obtained in this work for C$_2$C$_2$imTFSI deviate from the literature values, reported in a paper from Rocha et al. and Domanska et al. [42, 43] where they are less than 0.05% at the temperature $T =$ 298.15 K. A good agreement can be observed between the density values

with those reported by Rocha et al. [42], finding relative deviation in the whole temperature range from 0.01–0.05%. The relative deviation between the experimental values in this work and those published in the work of Tome et al. [41] is 0.8%. Comparing our viscosity results given in Table 2 with those obtained in the paper from Rocha et al. [42], it can be seen that deviation is 3–14%. The relative deviation between the experimental viscosity measured in this work and those reported in the literature at $T =$ 298.15 K is 8%. A good agreement can be observed between the values of electrical conductivity with those reported by Higarava et al. [44] finding a relative deviation in the temperature $T =$ 293.15 K, which is below 2.5%.

The comparison of density values obtained for C$_2$C$_2$imTFSI with ionic liquids C$_1$C$_1$imTFSI [47] and C$_1$C$_2$imTFSI [48] is presented in Fig. S4a. From Fig. S4a, it could be seen that density decreases as the alkyl chain length on the cation increases. It is understandable bearing in mind that the larger the individual ions are, the Coloumbic interactions would be weaker. Therefore, the ions are less closely packed, causing lower macroscopic density. Additionally, the cation symmetry provides a different structural organization which also allows the fine tuning of IL physicochemical properties [49, 50]. Xiao et al. [51] showed that the symmetric IL series presents a higher local order and higher intermolecular dynamics in frequency than the asymmetric series.

Figure 1a presents a comparison between physicochemical properties for pure ionic liquid and 0.5 mol dm^{-3} LiTFSI in C$_2$C$_2$imTFSI (LiTFSI/C$_2$C$_2$imTFSI electrolyte). From Fig. 1a, it can be seen that density increases with a dissolved lithium salt in C$_2$C$_2$imTFSI and decreases linearly with increasing temperature. Obtained data were fitted as a function of temperature using a linear fit, with parameters tabulated in Table S1. For experimental densities (Table 2, Fig. 1a) were used to derive other thermodynamic properties such as coefficient of thermal expansion [52–54] given in the supporting information of this manuscript (Fig. S5, Table S2).

The effect of temperature on the viscosity of C$_2$C$_2$imTFSI and LiTFSI/C$_2$C$_2$imTFSI electrolyte is graphically presented in Fig. 1b for the whole temperature range. The experimental results of viscosity at different temperatures were fitted using the Vogel–Fulcher–Tammann (VFT) equation [55–57]:

$$\eta = a\exp(b/(T-T\text{o})) \tag{1}$$

where η is the viscosity, T is the temperature in K and a, b, and T_{o} are the coefficients of VFT equation whose values are given in Table S3 together with the standard deviations. The temperature has a significant effect on the performances of the IL-containing batteries, as the viscosity is a crucial limitation [58].

From Fig. 1b, it can be seen that viscosity decreases 2–2.5 times when temperature increases in the range from 293.15 to

Table 2 Experimental and literature values of density, (*d*), viscosity, (*η*) and electrical conductivity, (*κ*), of the pure liquid C_2C_2imTFSI at the specified temperatures and atmospheric pressure (*p* = 0.1 MPa)

d/(g cm^{-3})			*η*/(mPa s)		*κ*/(mS cm^{-1})	
T/(K)	This work	References	This work	References	This work	References
293.15	1.48035	1.4692[a]; 1.4799[b]	38.09	36.89[a]; 36.00[d]; 35.00[f]	4.94	6.2[d]
298.15	1.47532	1.4632[a]; 1.4749[b]; 1.4760[c]; 1.452[d]; 1.470[e]	32.54	30.78[b]	5.81	–
303.15	1.47030	1.4577[a]; 1.4699[b]	28.04	26.02[b]	6.66	–
308.15	1.46516	1.4473[a]; 1.4650[b]	24.59	22.21[b]	7.57	–
313.15	1.45993	1.4600[b]	21.60	19.15[b]	8.33	–
318.15	1.45473	1.4551[b]	19.35	16.65[b]	9.23	–
323.15	1.44956	1.4502[b]	17.40	14.61[b]	10.14	–

Standard uncertainty: $u(d) = 9.75 \cdot 10^{-1}$ kg m^{-3}; $u_d(T) = 0.015$ K, $u_\eta(T) = 0.02$ K, relative standard uncertainties are $u_r(\eta) = 2\%$, %, $u(\kappa) = 1.5\%$, $u_r(p) = 1.5\%$

a = [22], b = [23], c = [24], d = [25], e = [26], f = [27]

323.15 K from pure ionic liquid to 0.5 mol·dm^{-3} Li$^+$ electrolyte, respectively. The addition of LiTFSI in the ionic liquid increases the viscosity of the mixture, which is more pronounced at lower temperatures. Structural changes in LiTFSI/C_2C_2imTFSI mixture upon the addition of LiTFSI lead to a structure that causes higher density and viscosity [59].

The increase of electrical conductivity with temp1111erature for ionic liquid is observed in Fig. 1c and is in accordance with the fact that electrical conductivity of the IL largely depends on the viscosity [60]. Electrical conductivity decreases when a LiTFSI salt is added to the ionic liquid (Fig. 1c). The reduction of the electrical conductivity is associated with the ionic interactions between the Li$^+$ and the IL anion, which increase the viscosity and result in larger complexes with lower mobility [61–64].

Electrical conductivity data obtained for 0.5 mol dm^{-3} LiTFSI/C_2C_2imTFSI electrolyte are qualitatively compared with other ionic liquid–based electrolytes with the optimal compositions for LIBs reported in the literature [65–69]. It is evident that ionic liquid based–electrolytes at compositions stated as "optimal" for LIBs (presented in Fig. S5), including electrolyte studied in this work, have comparable electrical conductivity, which is one of the parameters that govern the performance of the lithium-ion batteries.

The relationship between molar conductivity (based on the experimental electrical conductivity and density data) and viscosity of the ionic liquid, as well for LiTFSI/C_2C_2imTFSI electrolyte, is illustrated by the qualitative approach developed by Walden [70], defined as

$$\Lambda_m \cdot \eta^\alpha = K = \text{const} \tag{3}$$

where Λ_m is the molar conductivity and η^α is the viscosity of the ionic liquid (or LiTFSI/C_2C_2imTFSI electrolyte). The

exponent α is used to describe the decoupling of mobile ions [71]. This exponent is the slope of the logarithmic form of the Eq. (3), while log K is the intercept given as

$$\log\Lambda_m = \alpha \cdot \log(\eta^{-1}) + \log K \tag{4}$$

The Walden rule relates the ionic mobility represented by the equivalent conductivity Λ_m to the fluidity (η^{-1}) of the medium through which the ions move [72]. Figure 2 shows the Walden plots for some imidazolium-based ILs (which are similar on the basis of the structure with investigated one, such as $\{[C_nC_1\text{im}][NTf_2]; n = 1 \text{ and } 2\}$) and for LiTFSI/$C_1C_2$imTFSI electrolyte, with temperatures varying from 293.15 to 323.15 K [47]. These plots are placed below the "ideal" KCl line, which represents 0.01 mol dm^{-3} KCl aqueous solution known to be fully dissociated and to have ions of equal mobility [71]. Previous reports have shown that many pure ionic liquids lie below the reference line indicating incomplete ionization of these ionic liquids, as was explained by the Walden plot [70–73]. Deviation from the ideal line is commonly observed for most of ILs and is correlated to the partial Walden rule [72–74]. From Fig. 2, it can be seen that with the alkyl chain increase on cation of IL, Walden plot is on a larger distance from the ideal line. It indicates that pure ILs with longer alkyl side chains show lower ionization. It is important to evaluate the percent of ionization as a quantitative expression as ionicity (*I*), calculated with Eq. (5) [75, 76]:

$$I = 10^{-\left(\log(\eta^{-1}) - \log\Lambda_m\right)} \tag{5}$$

Ionicity of the C_2C_2imTFSI is calculated at *T* = 298.15 K and it is 53% in case of pure ionic liquid and 80% in case of LiTFSI/C_2C_2imTFSI electrolyte. A lithium salt addition to IL
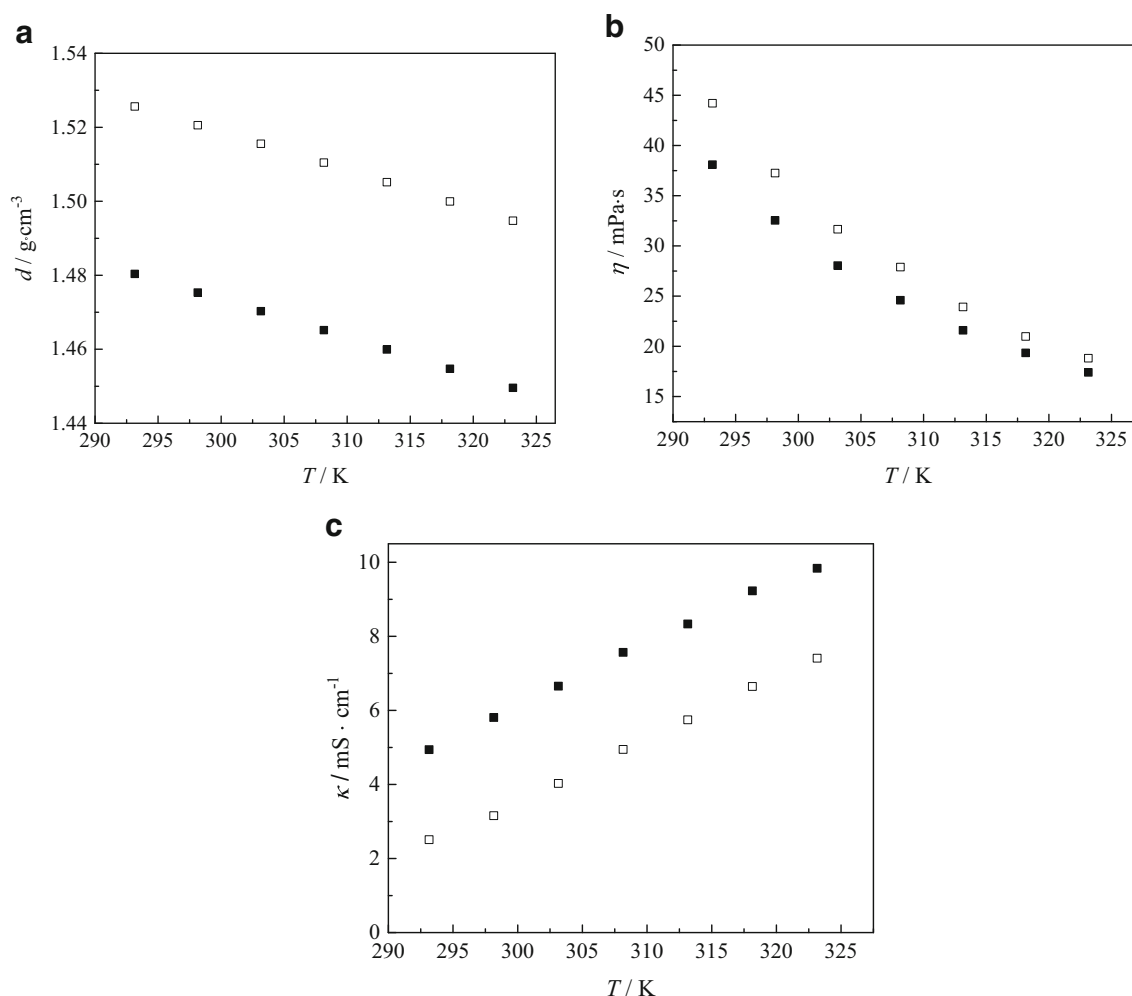
a

b

c

Fig. 1 Comparison of experimental: **a** density, (d), **b** viscosity, (η), and **c** electrical conductivity, (κ) for (■) C_2C_2imTFSI and (□) LiTFSI/C_1C_2imTFSI, as a function of temperature

usually reduces the ionicity because of the high charge density of lithium, and the Coulombic interaction was favoured and increases ion pairing [76].

In terms of electrolyte safety features, it is important to assess the flammability of LiTFSI/C_2C_2imTFSI electrolyte. The flame did not appear during heating of 120 s, and this is a clear indication that LiTFSI/C_2C_2imTFSI electrolyte is non-flammable (Fig. S6). Thus, LiTFSI/C_2C_2imTFSI (0.5 mol dm^{-3} LiTFSI in C_2C_2imTFSI) is selected as an electrolyte for the following electrochemical characterization of nanotubular anatase TiO$_2$ as anode material for LIBs.

Electrochemical characterisation

Cyclic voltammetry

Initially, the electrochemical stability window of LiTFSI/ C_2C_2imTFSI electrolyte, under non-atmospheric conditions [77], has been measured by cyclic voltammetry using a glassy carbon (GC) as working electrode. The cyclic

voltammograms obtained at a scan rate of 10 mV·s^{-1} are presented in Fig. 3 at T = 298.15 K. The voltage window between the onset of oxidation and reduction is around 4 V. It is important to emphasize that small amounts of water can narrow the potential limits of ionic liquids to a certain degree [77].

According to Fig. 3, Li$_4$Ti$_5$O$_{12}$ (LTO) and TiO$_2$ may be considered as suitable anode materials to be tested in LiTFSI/C_2C_2imTFSI as a potential electrolyte for Li-ion batteries. Despite the fact that LTO has slightly lower working potential, the choice fell on anatase TiO$_2$ NTs. The Ti/TiO$_2$ NT electrode, obtained by anodic oxidation, concurrently joins the current collector and the active material without the binder and therefore is more robust for measurements at elevated temperatures in bottle-type cells.

Figure 4a shows CVs recorded for anatase TiO$_2$ NTA electrode in LiTFSI/C_2C_2imTFSI electrolyte at scan rates 1, 2 and 5 mV·s^{-1} at temperature T = 298.15 K. In all cases, the potential was scanned from 3 to 1 V and then vice versa. At all scan rates, Ti^{4+}/Ti^{3+} redox peaks appear owing to the process of insertion/extraction of Li$^+$ and may be considered fast most
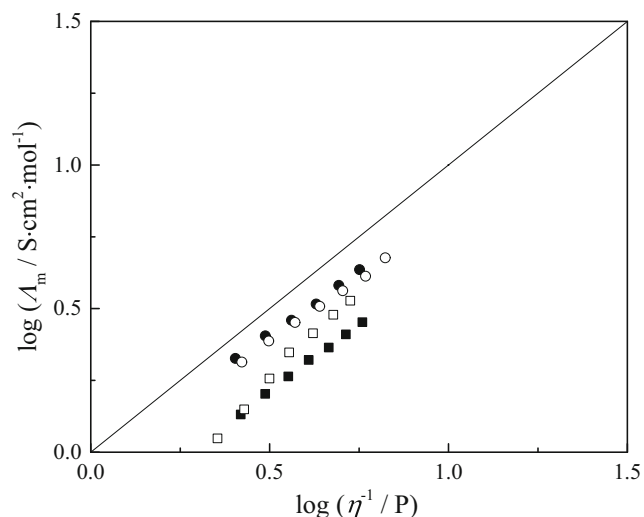
Fig. 2 Walden plot (Eq. 4) for (■) $C_2C_2imTFSI$, () $C_1C_2imTFSI$ [29], (●) $C_1C_1imTFSI$ [28] and (□) LiTFSI/$C_2C_2imTFSI$ electrolyte

likely due to the short diffusion length of Li^+ ion into nanotube walls. At all scan rates, the common appearance of CVs was obtained, i.e. a higher scan rate gives a higher current peak, except the peak heights at 1 and 2 mV s^{-1} in reduction are the same. This happened because during a reduction in scan rate 1 mV s^{-1}, the lithium ions where for the first time inserted into TiO$_2$ NTs and some of them remained irreversibly bounded (irreversible capacity loss). The smaller peak, more clearly visible in reduction at all scan rates, most likely may be attributed to the additional filling of oxygen octahedra above composition $Li_{0.5}TiO_2$ [78]. At the lowest scan rate of 1 mV·s^{-1} (Fig. 4b), redox peak-to-peak separation is 0.441 V and is similar to that observed for IL-based electrolytes [19, 20], and also for LiPF$_6$/EC-DMC [79] and LiClO$_4$/PC [80] electrolyte.

Figure 4b demonstrates the influence of temperature on CVs recorded at a scan rate 5 mV·s^{-1}. The increase in temperature at the same time enhances the height of the redox peaks and decreases the peak-to-peak separation. This indicates the significant improvement of both lithium-ion storage capability and reversibility of the Ti/TiO$_2$ NT electrode. Although CVs were recorded by using the CI method which eliminates electrolyte resistance, the peak-to-peak separation, even at the highest temperature $T = 328.15$ K, is significantly larger from the Nernstian. The main reason is most likely the slow electron transport inside the TiO$_2$ NTs even though lithium intercalation reduces the energy gap of anatase TiO$_2$ semiconductor [34].

Galvanostatic experiments

The galvanostatic (GS) cycling for the first Ti/TiO$_2$ NTA electrode was performed by using the current density of 100 μA cm^{-2} at different temperatures. The current rate was

calculated later by scraping nanotubes from the Ti foil. The galvanostatic charge/discharge (lithium extraction/lithium insertion) capacity of TiO$_2$ NTs is shown for 150 cycles in Fig. 5a for LiTFSI/$C_2C_2imTFSI$ electrolyte, at different temperatures. After initial capacity drop, the insertion/extraction capacity of Li^+ ion into/from TiO$_2$ NTs became very stable at $T = 298.15$ K. After 50 cycles at this temperature, the insertion/extraction capacity amounted 111.2/109.5 mAh g^{-1}. This corresponds to the Coulombic efficiency of 98.5%. By increasing temperature from 298.15 to 308.15 K, capacity significantly rises, but is in the constant slow decrease. After 25 cycles at temperature $T = 308.15$ K, insertion/extraction capacity was 173.1/164.4 mAh·g^{-1}, which gives, comparing with previous temperature, the lower Coulombic efficiency of 95.0%.

The growth of temperature to $T = 318.15$ K, leads to a further jump in capacity. At this temperature, the capacity drop is much steeper in the first ~ 11 cycles with Coulombic efficiency which is between 92.2% for the 1st (76th in total) and 95.2% for the 11th (86th in total) cycle. Then, both in charge and discharge, capacity decreases to some extent, but Coulombic efficiency increases and capacity drop is significantly diminished. At the end of cycling at $T = 318.15$ K, for the 25th (100th in total) cycle, the insertion/extraction capacity is 211.4/207.1 mAh g^{-1} and Coulombic efficiency 98.0%. The $T = 328.15$ K is the highest temperature at which galvanostatic cycling was examined. Very stable cycling behaviour was obtained in this case. From a total of 25 cycles, in the last 10 cycles practically, there is no capacity fade. For the last 25th (125th in total) cycle, insertion/extraction capacity of Li^+ is 253.5/251.5 mAh g^{-1}, and Coulombic efficiency is as high as 99.2%. These experimental facts, most likely, indicate the formation of a film on the surface of TiO$_2$ NTs which was more or less accomplished at $T = 318.15$ K and prevented
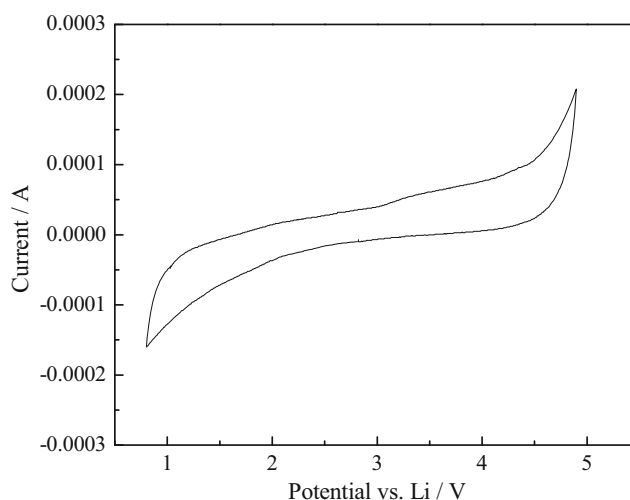

Fig. 3 Electrochemical stability window of LiTFSI/$C_2C_2imTFSI$ electrolyte obtained at room temperature by using a glassy carbon (GC) working electrode and Li-metal foil as both counter and a reference electrode. The scan rate was 10 mV s^{-1}
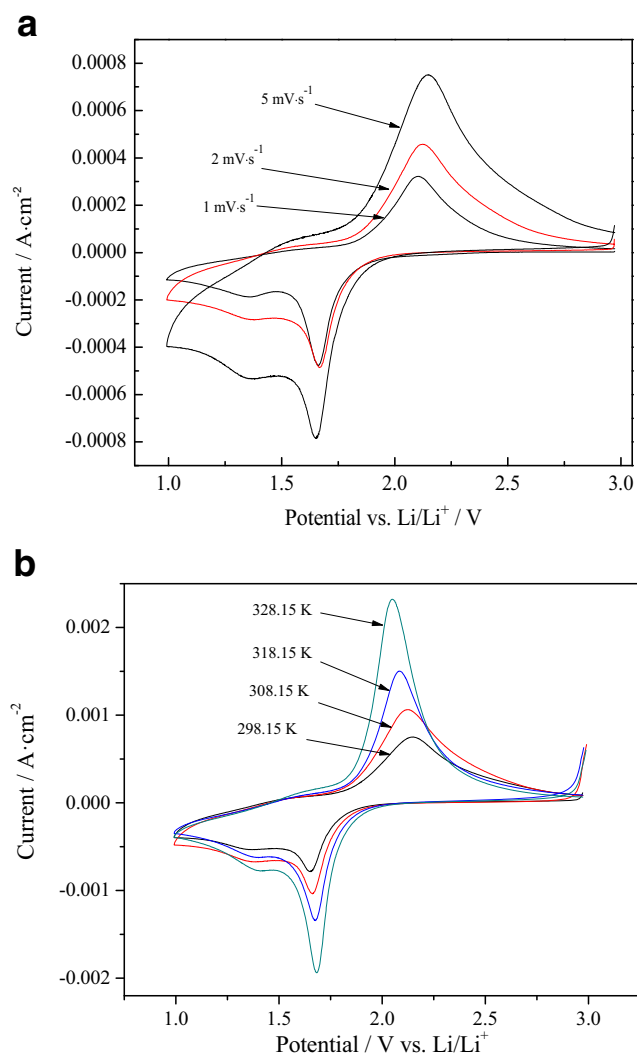
Fig. 4 Cyclic voltammograms of anatase TiO$_2$ NTAs in LiTFSI/C$_2$C$_2$imTFSI electrolyte recorded at **a** different scan rates 1, 2 and 5 mV·s^{-1} at $T = 298.15$ K and **b** different temperatures (298.15–328.15) K at scan rate 5 mV·s^{-1}

NTs. During the first 250 cycles, the current rate was changed every 50 cycles, and the next 250 cycles current rate was constant and the same as at the beginning of cycling, Fig. 5b. The capacity and Coulombic efficiency follow a similar trend during a current rate decrease, Fig. 5b, as with temperature increase, Fig. 5a. By decreasing the current rate from 2.76 to 1.38 C charge/discharge capacity increases and Coulombic efficiency slightly decreases. Further decrease of the current rate to 0.69 C initially decreases Coulombic efficiency, but at the end of cycling at this current rate, charge and discharge capacity become stabilized and Coulombic efficiency attains 100%. During further cycling, at higher current rates, it remains at maximum level of 100%. During the last 250 cycles at a current rate of 2.76 C, capacity fade is around 4%. Most likely, the formation of the film at the surface of electrode is completed at a current rate of 0.69 C. After 500 cycles at RT, the colour of the electrolyte became bright yellow (Fig. S7).
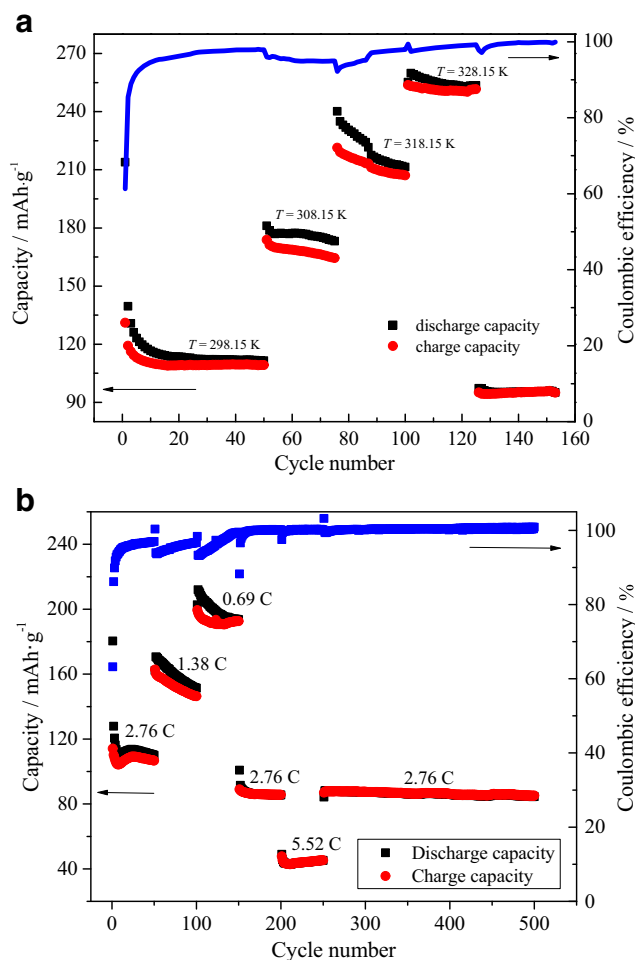
Fig. 5 Charge/discharge performance of anatase TiO$_2$ NTAs in LiTFSI/C$_2$C$_2$imTFSI electrolyte at **a** different temperatures at a current rate of 3 C and **b** different current rates: 0.69 C, 1.38 C, 2.76 C and 5.52 C at room temperature
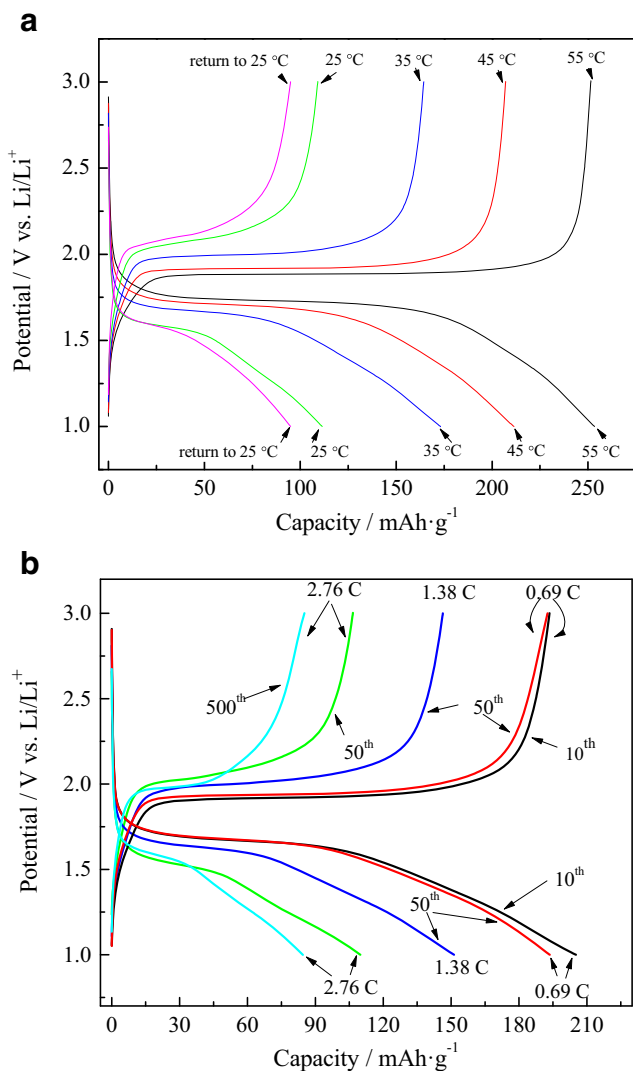
further decomposition of the electrolyte. Because of this, cycling behaviour at $T = 328.15$ K was very stable and with very high Coulombic efficiency. The cycling behaviour after returning to $T = 298.15$ K is in favour of film formation. Namely, even though insertion/extraction capacity declines (95.7/95.6 mAh g^{-1} for the 150th cycle), compared with capacities in the first 50 cycles, cycling behaviour from the 125th to 150th cycle may be considered exceptionally stable with no capacity drop and Coulombic efficiency as high as 99.9%. The change in colour of electrolyte from colourless to pale yellow indicates the existence of electrolyte decomposition, as shown in Fig. S7.

The second Ti/TiO$_2$ NTA electrode was GS cycled at different current densities (in orders 100, 50, 25, 100, 200 and finally 100 μA cm^{-2}) at room temperature (RT) (Fig. 5b). Current rates were calculated from the mass of

Fig. 6 Charge/discharge voltage profiles for anatase TiO_2 NTAs in LiTFSI/C_2C_2imTFSI electrolyte at **a** different temperatures and at a rate of 3 C and **b** different current rates 0.69 C, 1.38 C, 2.76 C and 5.52 C at room temperature

Voltage profiles

The real theoretical capacity of TiO_2 should be 335 mAh g^{-1}, but actual theoretical capacity is usually taken to be 167.5 mAh g^{-1}, which corresponds to composition $Li_{0.5}TiO_2$ in which Li$^+$ ion occupies the half of octahedral cites. However, it had been demonstrated that for very small particles, capacity can be larger [23]. Figure 5a shows that charge/discharge capacity of anatase TiO_2 NTAs, at a high current rate, may also exceed theoretical value. Figure 6a depicts voltage profiles in the charge and discharge for temperatures 298.15–328.15 K. Every voltage profile in discharge (lithium insertion) has three distinct regions. The first region is from 3 V down to the constant voltage plateau, which presents the second region, and the third region is from plateau down to 1 V. The first region is rather ascribed to electric double-layer

capacitance than to the formation of solid solution domain of TiO_2 and Li_xTiO_2 [81]. The region where the voltage is constant reflects coexistence of two phases: Li-poor $Li_{0.026}TiO_2$ and Li-rich $Li_{-0.55}TiO_2$. The region with inclined voltage profile down to 1 V designates the existence of surface storage mechanism which leads to pseudo-capacitive behaviour [81–83]. Figure 6 a shows that values of the overall capacity of anatase TiO_2 NTAs, which exceeds theoretical capacity, come from the large contribution of lithium surface storage capacity, which does not depend on bulk diffusion time. The relative contribution of surface storage capacity decreases with the temperature increase because of the increased diffusion coefficient of lithium-ion [37, 38], but remains significant. The decrease in the difference between voltage plateaus in charge and discharge with the temperature increase shows the expected diminution of overall resistance of the cell at higher temperatures. The enlargement of difference between plateaus after returning to $T = 298.15$ K confirms the findings of EIS about the increase of overall resistance due to the increase of resistance of the electrolyte, formation of the film and the increase in charge transfer resistance. The decrease in capacity after returning to $T = 298.15$ K may come from the partial blocking of pores of NTs with solid products of electrolyte decomposition which can reduce the number of sites for lithium insertion.

Figure 6b shows voltage profiles during charging and discharging at room temperature at different current rates. The influence of the decrease of the current rate on voltage profiles is expected to be similar to the influence of the temperature increase: capacity increases and the difference between voltage plateaus become smaller. After 50 cycles, at the lowest current rate of 0.69 C at which the uppermost jump in Coulombic efficiency happens, the difference between voltage profiles in charge and discharge slightly increases comparing with 10th cycle. This shows a small increase of resistivity in the system which, having in mind achieved Coulombic efficiency of 100% may be attributed to film formation, as suggested above in the text. Figure 6b also shows voltage profiles after 500 cycles in total, from which last 250 cycles are at current rate of 2.76 C, in comparison with profiles at the same current rate after 50 cycles. It can be seen that cycling between the 50th and 500th cycle at different current rates significantly decreases capacity. If we assume that there is no loss of active material of robust Ti/TiO_2 NTA electrode, this decrease may be attributed to blocking some of NT sites for lithium insertion with products of electrolyte decomposition, most likely deeper inside NTs. The difference in voltage profiles in charge and discharge, at the same time, after 500 cycles becomes smaller then after 50 cycles. This indicates, in the first place, the decrease in film and charge transfer resistance during cycling at different rates.

FTIR, Raman and UV-VIS spectra of solutions after GS cycling were recorded, having in mind the observed change

from colourless to yellow colour. Only some minor changes were observed in FTIR spectra, and there were no changes in Raman spectra of these solutions in comparison with initial IL-based electrolyte. UV-Vis spectra showed the strong absorption of formed compound(s), which must be present in very small concentration, undetectable with vibrational spectroscopy (Figs. S8–S10).

Impedance measurements

In order to confirm the formation of film on the electrode surface, impedance measurements were performed for the electrode which is subjected to GS cycling at different temperatures. EIS spectra were recorded after 50 cycles at $T = 298.15$ K, and after 150 cycles, again at $T = 298.15$ K, after the cell was subjected to galvanostatic charge/discharge regime at elevated temperatures (Fig. 5). After 50 cycles, in
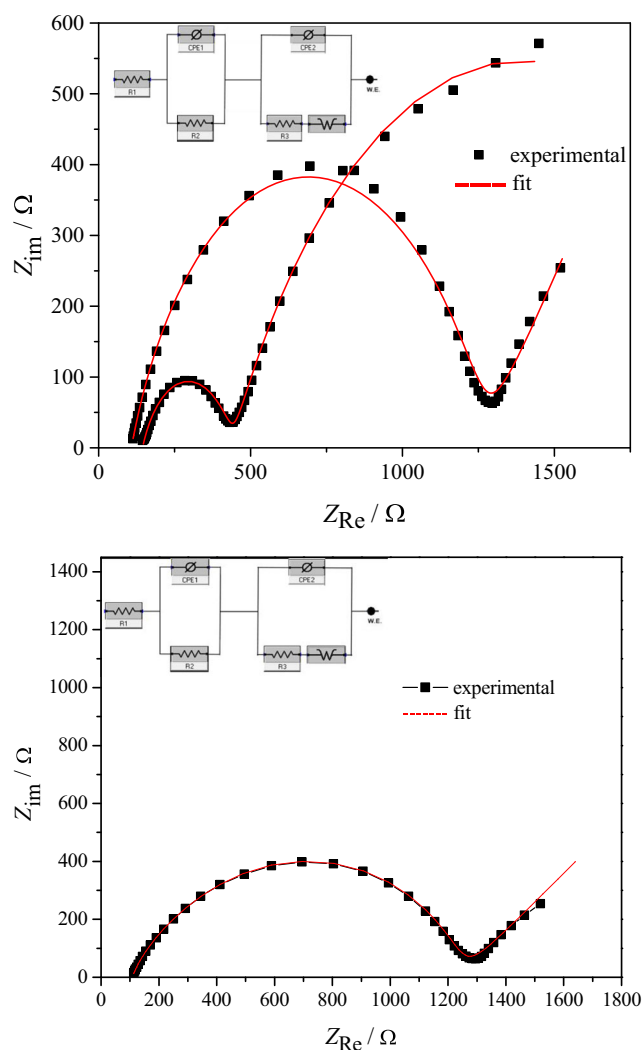

Fig. 7 Nyquist plots obtained using electrochemical impedance spectroscopy for LiTFSI/C₂C₂imTFSI. The inset shows a circuit equivalent to the systems under consideration

the Nyquist plot, impedance data form a depressed semicircle in a high- and middle-frequency region and unit slope line in a low-frequency region, Fig. 7 The semicircle can be fitted to two depressed semicircles, corresponding to film and charge transfer impedance and unit slope line is due to Warburg impedance. The film resistance, in this case, is much smaller from charge transfer resistance. After 150 cycles, two distinct semicircles can be observed in the Nyquist plot. The first semicircle is due to the film formed on the surface of TiO₂ NTs during cycling at elevated temperatures, and the second semicircle to charge transfer process. Although more data at lower frequencies are missing for a more accurate fit, it may be concluded that both film and charge transfer resistance are increased after 150 cycles at different temperatures. Linear part in impedance plot is missing at low frequencies meaning that the process of lithium insertion/deinsertion is under kinetic control. The intercept of a semicircle with x-axis in the high-frequency region, in both cases, gives the resistance of electrolyte, which is changed to some extent after cycling at elevated temperatures. Finally, EIS confirmed the formation of film on electrode surface which, according to GS cycling experiments, was formed as a result of reductive decomposition of electrolyte. Most likely C₂C₂im⁺ ion is reduced at electrode surface, but that remains to be confirmed.

Conclusions

The density, viscosity and electrical conductivity data were obtained at different temperatures for ionic liquid C₂C₂imTFSI as well as for 0.5-M solution of LiTFSI in C₂C₂imTFSI. The electrochemical properties of the LiTFSI/C₂C₂imTFSI system as a potential electrolyte for LIBs were tested by using anatase TiO₂ nanotube array electrode as anode material. Despite the low vapour pressure, non-flammability and room temperature electrochemical stability of ionic liquid–based electrolytes, which indicates their possible use in safer LIBs, the need for their testing at elevated temperatures was emphasized. In the case of LiTFSI/C₂C₂imTFSI electrolyte, electrochemical experiments at elevated temperatures up to $T = 328.15$ K not only showed the significant improvement in Li⁺ storage capability into Ti/TiO₂ NTAs electrode but also leads to the reductive decomposition of the electrolyte. Finally, such decomposition leads to the formation of a film on the electrode which significantly improves Coulombic efficiency but increases electrolyte and charge transfer resistance and decrease charge/discharge capacity of TiO₂ electrode at $T = 298.15$ K compared with the values before cycling at higher temperatures.

Compliance with ethical standards

Conflict of interest   The authors declare that they have no conflict of interest.

References

1. Aurbach D, Markovsky B, Salitra G, Markevich E, Talyossef Y, Koltypin M, Nazar L, Ellis B, Kovacheva D (2007) Review on electrode–electrolyte solution interactions, related to cathode materials for Li-ion batteries. J Power Sources 165:491–499. https://doi.org/10.1016/j.jpowsour.2006.10.025

2. Kawamura T, Kimura A, Egashira M, Okada S, Yamaki J (2002) Thermal stability of alkyl carbonate mixed-solvent electrolytes for lithium ion cells. J Power Sources 104:260–264. https://doi.org/10.1016/S0378-7753(01)00960-0

3. Eshetu GG, Bertrand J-P, Lecocq A, Grugeon S, Laruelle S, Armand M, Marlair G (2014) Fire behavior of carbonates-based electrolytes used in Li-ion rechargeable batteries with a focus on the role of the $LiPF_6$ and LiFSI salts. J Power Sources 269:804–811. https://doi.org/10.1016/j.jpowsour.2014.07.065

4. Wang Q, Ping P, Zhao X, Chu G, Sun J, Chen C (2012) Thermal runaway caused fire and explosion of lithium ion battery. J Power Sources 208:210–224. https://doi.org/10.1016/j.jpowsour.2012.02.038

5. Diallo AB, Morgan AB, Len C, Marlair G (2013) An innovative experimental approach aiming to understand and quantify the actual fire hazards of ionic liquids. Energy Environ Sci 6:699–710. https://doi.org/10.1039/C2EE23926D

6. Guerfi A, Dontigny M, Charest P, Petitclerc M, Lagacé M, Vijh A, Zaghib K (2010) Improved electrolytes for Li-ion batteries: mixtures of ionic liquid and organic electrolyte with enhanced safety and electrochemical performance. J Power Sources 195:845–852. https://doi.org/10.1016/j.jpowsour.2009.08.056

7. Fernicola A, Croce F, Scrosati B, Watanabe T, Ohno H (2007) LiTFSI-BEPyTFSI as an improved ionic liquid electrolyte for rechargeable lithium batteries. J Power Sources 174:342–348. https://doi.org/10.1016/j.jpowsour.2007.09.013

8. Cho E, Mun J, Chae OB, Kwon OM, Kim H-T, Ryu JH, Kim YG, Oh SM (2012) Corrosion/passivation of aluminum current collector in bis(fluorosulfonyl)imide-based ionic liquid for lithium-ion batteries. Electrochem Commun 22:1–3. https://doi.org/10.1016/j.elecom.2012.05.018

9. Peng C, Yang L, Zhang Z, Tachibana K, Yang Y (2007) Anodic behavior of Al current collector in 1-alkyl-3-methylimidazolium bis[(trifluoromethyl)sulfonyl] amide ionic liquid electrolytes. J Power Sources 173:510–517. https://doi.org/10.1016/j.jpowsour.2007.05.006

10. Bazito FFC, Kawano Y, Torresi RM (2007) Synthesis and characterization of two ionic liquids with emphasis on their chemical stability towards metallic lithium. Electrochim Acta 52:6427–6437. https://doi.org/10.1016/j.electacta.2007.04.064

11. Olschewski M, Gustus R, Marschewski M, Hoefft O, Endres F (2014) Spectroscopic characterization of the interaction of lithium with thin films of the ionic liquid 1-octyl-3-methylimidazolium bis(trifluoromethylsulfonyl)amide. Phys Chem Chem Phys 16:25969–25977. https://doi.org/10.1039/C4CP03091E

12. Mun J, Jung Y, Yim T, Lee H, Kim H, Kim Y, Oh S (2009) Electrochemical stability of bis(trifluoromethanesulfonyl)imide-based ionic liquids at elevated temperature as a solvent for a titanium oxide bronze electrode. J Power Sources 194:1068–1074. https://doi.org/10.1016/j.jpowsour.2009.05.048

13. Shimizu M, Usui H, Matsumoto K, Nokami T, Itoh T, Sakaguchi H (2014) Effect of cation structure of ionic liquids on anode properties of Si electrodes for LIB. J Electrochem Soc 161:A1765–A1771. https://doi.org/10.1149/2.0021412jes

14. Choi J-A, Kim D-W, Bae Y-S, Song S-W, Hong S-H, Lee S-M (2011) Electrochemical and interfacial behavior of a $FeSi_{2.7}$ thin film electrode in an ionic liquid electrolyte. Electrochim Acta 56:9818–9823. https://doi.org/10.1016/j.electacta.2011.08.080

15. Srour H, Chancelier L, Bolimowska E, Gutel T, Mailley S, Rouault H, Santini CC (2015) Ionic liquid-based electrolytes for lithium-ion batteries: review of performances of various electrode systems. J Appl Electrochem 46:149–155. https://doi.org/10.1007/s10800-015-0905-1

16. Tachikawa N, Park JW, Yoshida K, Tamura T, Dokko K, Watanabe M (2010) Limiting current density in ionic liquid electrolyte for lithium batteries. Communication 78:342–352. https://doi.org/10.5796/electrochemistry.78.349

17. Seki S, Kobayashi Y, Miyashiro H, Ohno Y, Usami A, Mita Y, Kihira N, Watanabe M, Terada N (2006) Lithium secondary batteries using modified-imidazolium room-temperature ionic liquid. J Phys Chem B 110:10228–10230. https://doi.org/10.1021/jp0620872

18. MacFarlane DR, Tachikawa N, Forsyth M, Pringle JM, Howlett PC, Elliott GD, Davis JH, Watanabe M, Simon P, Angell CA (2014) Energy applications of ionic liquids. Energy Environ Sci 7:232–250. https://doi.org/10.1039/c3ee42099j

19. Wang Z, Cai Y, Dong T, Chen S, Lu X (2013) Triethylbutylammonium bis(trifluoromethane-sulphonyl)imide ionic liquid as an effective electrolyte additive for Li-ion batteries. Ionics 19:887–894. https://doi.org/10.1007/s11581-012-0820-y

20. Fernicola A, Scrosati B, Ohno H (2006) Potentialities of ionic liquids as new electrolyte media in advanced electrochemical devices. Ionics 12:95–102. https://doi.org/10.1007/s11581-006-0023-5

21. Roy P, Berger S, Schmuki P (2011) TiO_2 nanotubes: synthesis and applications. Angew Chem Int Ed 50:2904–2939. https://doi.org/10.1002/anie.201001374

22. Mor GK, Shankar K, Paulose M, Varghesen OK, Grimes CA (2006) Use of highly-ordered TiO_2 nanotube arrays in dye-sensitized solar cells. Nano Lett 6:215–218. https://doi.org/10.1021/nl052099j

23. Meekins BH, Kamat PV (2009) Got TiO_2 nanotubes? Lithium ion intercalation can boost their photoelectrochemical performance. ACS Nano 3:3437–3446. https://doi.org/10.1021/nn900897r

24. Park SG, Yang JJ, Rho JW, Kim HI, Habazaki H (2014) Electrochemical behavior of TiO_2 nanotube/Ti prepared by anodizing for micro-lithium ion batteries. J Korean Electrochem Soc 17:13–17. https://doi.org/10.5229/JKES.2014.17.1.13

25. Ling L, Bai Y, Li Y, Ni Q, Wang Z, Wu F, Wu C (2017) Quick activation of nanoporous anatase TiO_2 as high-rate and durable anode materials for sodium-ion batteries. ACS Appl Mater Interfaces 9:39432–39440. https://doi.org/10.1021/acsami.7b13927

26. Yan D, Yu C, Zhang X, Li J, Li J, Lu T, Pan L (2017) Enhanced electrochemical performances of anatase TiO_2 nanotubes by synergetic doping of Ni and N for sodium-ion batteries. Electrochim Acta 254:130–139. https://doi.org/10.1016/j.electacta.2017.09.120

27. Liu S, Luo Z, Tian G, Zhu M, Cai Z, Pan A, Liang S (2017) TiO_2 nanorods grown on carbon fiber cloth as binder-free electrode for sodium-ion batteries and flexible sodium-ion capacitors. J Power Sources 363:284–290. https://doi.org/10.1016/j.jpowsour.2017.07.098

28. Xu Y, Lotfabad EM, Wang H, Farbod B, Xu Z, Kohandehghan A, Mitlin D (2013) Nanocrystalline anatase TiO_2: a new anode material for rechargeable sodium ion batteries. Chem Commun 49:8973–8975. https://doi.org/10.1039/C3CC45254A

29. Usui H, Yoshioka S, Wasada K, Shimizu M, Sakaguchi H (2015) Nb-doped rutile TiO_2: a potential anode material for Na-ion battery. ACS Appl Mater Interfaces 7:6567–6573. https://doi.org/10.1021/am508670z

30. Wang J, Zhao H, Li Z, Wen Y, Xia Q, Zhang Y, Yushin G (2016) Revealing rate limitations in nanocrystalline $Li_4Ti_5O_{12}$ anodes for high-power Lithium ion batteries. Adv Mater Technol 1:1600003. https://doi.org/10.1002/admi.201600003

31. Bella F, Muñoz-García AB, Meligrana G, Lamberti A, Destro M, Pavone M, Gerbaldi C (2017) Unveiling the controversial mechanism of reversible Na storage in TiO_2 nanotube arrays: amorphous versus anatase TiO_2. Nano Res 10:2891–2903. https://doi.org/10.1007/s12274-017-1656-6

32. Bella F, Muñoz-García AB, Colò F, Meligrana G, Lamberti A, Destro M, Pavone M, Gerbaldi C (2018) Combined structural, chemometric, and electrochemical investigation of vertically aligned TiO_2 nanotubes for Na-ion batteries. ACS Omega 3:8440–8450. https://doi.org/10.1021/acsomega.8b01117

33. Bella F, Lamberti A, Bianco S, Tresso E, Gerbaldi C, Pirri CF (2016) Floating, flexible polymeric dye-sensitized solar-cell architecture: the way of near-future photovoltaics. Adv Mater Technol 1:1–9. https://doi.org/10.1002/admt.201600002

34. Abate A, Correa-Baena J-P, Saliba M, Suait MS, Bella F (2018) Perovskite solar cells: from the laboratory to the assembly line. Chem Eur J 24:1–19. https://doi.org/10.1002/chem.201704507

35. Zhou H, Zhang Y (2014) Electrochemically self-doped TiO_2 nanotube arrays for supercapacitors. J Phys Chem C 118:5626–5636. https://doi.org/10.1021/jp4082883

36. Yu C, Wang Y, Zheng H, Zhang J, Yang W, Shu X, Qin Y, Cui J, Zhang Y, Wu Y (2017) Supercapacitive performance of homogeneous Co_3O_4/TiO_2 nanotube arrays enhanced by carbon layer and oxygen vacancies. J Solid State Electrochem 21:1069–1078. https://doi.org/10.1007/s10008-016-3441-y

37. Papović S, Cvjetićanin N, Gadžurić S, Bešter-Rogač M, Vraneš M (2017) Physicochemical and electrochemical characterisation of imidazolium based IL + GBL mixtures as electrolytes for lithium-ion batteries. Phys Chem Chem Phys 19:28139–28152. https://doi.org/10.1039/C7CP04478J

38. Zec N, Cvjetićanin N, Bešter-Rogač M, Vraneš M, Gadžurić S (2017) Electrochemical performance of anatase TiO_2 nanotube arrays electrode in ionic liquid based electrolyte for lithium ion batteries. J Electrochem Soc 164:H5100–H5107. https://doi.org/10.1149/2.0051708jes

39. Macak JM, Hildebrand H, Marten-Jahns U, Schmuki P (2008) Mechanistic aspects and growth of large diameter self-organized TiO_2 nanotubes. J Electroanal Chem 621:254–266. https://doi.org/10.1016/j.jelechem.2008.01.005

40. Hamelin J, Bose TK, Thoen J (1990) Dielectric constant and the electric conductivity near the consolute point of the critical binary liquid mixture nitroethane–3-methylpentane. Phys Rev A 42:4735–4742. https://doi.org/10.1103/PhysRevA.42.4735

41. Tomé LIN, Catambas VR, Teles ARR, Freire MG, Marrucho IM, Coutinho JAP (2016) Tryptophan extraction using hydrophobic ionic liquids. Sep Purif Technol 72:167–173. https://doi.org/10.1016/j.seppur.2010.02.002

42. Rocha MAA, Neves CMSS, Freire MG, Russina O, Triolo A, Coutinho JAP, Santos LMNF (2013) Alkylimidazolium based ionic liquids: impact of cation symmetry on their nanoscale structural organization. 117:10889–10897. https://doi.org/10.1021/jp406374a

43. Domańska U, Rekawek A, Marciniak A (2008) Solubility of 1-alkyl-3-ethylimidazolium-based ionic liquids in water and 1-octanol. J Chem Eng Data 53:1126–1132. https://doi.org/10.1021/je700693z

44. Hagiwara R, Ito Y (2000) Room temperature ionic liquids of alkylimidazolium cations and fluoroanions. J Fluor Chem 105:221–227. https://doi.org/10.1016/S0022-1139(99)00267-5

45. Ye C, Sheeve JM (2007) Rapid and accurate estimation of densities of room-temperature ionic liquids and salts. J Phys Chem 111:1456–1461. https://doi.org/10.1021/jp066202k

46. Bonhôte P, Dias A-P, Papageorgiou N, Kalyanasundaram K, Grätzel M (1996) Hydrophobic. Highly conductive ambient-temperature molten salts. Inorg Chem 35:1168–1178. https://doi.org/10.1021/ic951325x

47. Papović S, Gadžurić S, Bešter-Rogač M, Jović B, Vraneš M (2018) A systematic study on physicochemical and transport properties of imidazolium-based ionic liquids with γ-butyrolactone. J Chem Thermodyn 116:330–340. https://doi.org/10.1016/j.jct.2017.10.004

48. Papović S, Bešter-Rogač M, Vraneš M, Gadžurić S (2016) The effect of the alkyl chain length on physicochemial features of ionic liquids + γ-butyrolactone binary mixtures. J Chem Thermodyn 99:1–10. https://doi.org/10.1016/j.jct.2016.03.034

49. Zheng W, Mohammed A, Hines LG, Xiao D, Martinez OJ, Bartsch RA, Simon SL, Russina O, Triolo A, Quitevis EL (2011) Effect of cation symmetry on the morphology and physicochemical properties of imidazolium ionic liquids. J Phys Chem B 115:6572–6584. https://doi.org/10.1021/jp1115614

50. Dzyuba SV, Bartsch RA (2001) New room-temperature ionic liquids with C_2-symmetrical imidazolium cation. Chem Commun 0:1466–1467. https://doi.org/10.1039/b104512c

51. Xiao D, Hines LG, Li S, Bartsch RA, Quitevis EL (2009) Effect of cation symmetry and alkyl chain length on the structure and intermolecular dynamics of 1,3-dialkylimidazolium *bis*(-trifluoromethanesulfonyl)amide ionic liquids. J Phys Chem B 113:6426–6433. https://doi.org/10.1021/jp8102595

52. Muhammad A, Abdul Mutalib MI, Wilfred CD, Murugesan T, Shafeeq A (2008) Thermophysical properties of 1-hexyl-3-methyl imidazolium based ionic liquids with tetrafluoroborate, hexafluorophosphate and *bis*(trifluoromethylsulfonyl)imide anions. J Chem Thermodyn 40:1433–1438. https://doi.org/10.1016/j.jct.2008.04.016

53. Pereiro AB, Legido JL, Rodríguez A (2007) Physical properties of ionic liquids based on 1-alkyl-3-methylimidazolium cation and hexafluorophosphate as anion and temperature dependence. J Chem Thermodyn 39:1168–1175. https://doi.org/10.1016/j.jct.2006.12.005

54. Yunus NM, Abdul Mutalib MI, Man Z, Bustam MA, Murugesan T (2010) Thermophysical properties of 1-alkylpyridinum *bis*(-trifluoromethylsulfonyl)imide ionic liquids. J Chem Thermodyn 42:491–495. https://doi.org/10.1016/j.jct.2009.11.004

55. Vogel H (1921) The law of the relationship between viscosity of liquids and the temperature. Phys Z 22:645–646. https://doi.org/10.1155/2013/240571

56. Fulcher GS (1925) Analysis of recent data of the viscosity of glasses. J Am Ceram Soc 8:339–355. https://doi.org/10.1111/j.1151-2916.1925.tb16731.x

57. Tammann G, Hesse W (1926) Die Abhängigkeit der viscosität von der temperatur bie unterkühlten flüssigkeiten. Z Anorg Allg Chem 156:245–257. https://doi.org/10.1002/zaac.19261560121

58. Lewandowski A, Świderska-Mocek A (2009) Ionic liquids as electrolytes for Li-ion batteries–an overview of electrochemical studies. J Power Sources 194:601–609. https://doi.org/10.1016/j.jpowsour.2009.06.089

59. Monteiro MJ, Bazito FFC, Siqueira LJA, Ribeiro MCC, Torresi RM (2008) Transport coefficients, Raman spectroscopy, and computer simulation of lithium salt solutions in an ionic liquid. J Phys Chem B 112:2102–2109. https://doi.org/10.1021/jp077026y

60. Seddon KR, Stark A, Torres MJ (2000) Influence of chloride, water, and organic solvents on the physical properties of ionic liquids.

Pure Appl Chem 72:2275–2287. https://doi.org/10.1351/pac200072122275

61. Kim J-K, Lim D-H, Scheers J, Pitawala J, Wilken S, Johansson P, Ahn J-H, Matic A, Jacobsson PJ (2011) Properties of *N*-butyl-*N*-methylpyrrolidinium *Bis*(trifluoromethanesulfonyl) Imide Based Electrolytes as a Function of Lithium *Bis*(trifluoromethanesulfonyl) Imide Doping J Korean. Electrochem Soc 14:92–97. https://doi.org/10.5229/JKES.2011.14.2.092

62. Borodin O, Smith GD, Henderson W (2006) Li⁺ cation environment, transport, and mechanical properties of the LiTFSI doped *N*-methyl-N-alkylpyrrolidinium⁺ TFSI⁻ ionic liquids. J Phys Chem B 110:16879–16886. https://doi.org/10.1021/jp061930t

63. Lassègues J-C, Grondin J, Aupetit C, Johansson P (2009) Spectroscopic identification of the lithium ion transporting species in LiTFSI-doped ionic liquids. J Phys Chem A 113:305–314. https://doi.org/10.1021/jp806124w

64. Seo DM, Borodin O, Han S, Boyle PD, Henderson WJ (2012) Electrolyte solvation and ionic association II. Acetonitrile-lithium salt mixtures: highly dissociated salts. J Electrochem Soc 159:A1489–A1500. https://doi.org/10.1149/2.035209jes

65. Chagnes A, Diaw M, Carre B, Willmann P, Lemordant D (2005) Imidazolium-organic solvent mixtures as electrolytes for lithium batteries. J Power Sources 145:82–88. https://doi.org/10.1016/j.jpowsour.2004.12.035

66. Montanino M, Carewska M, Alessandrini F, Passerini S, Appetecchi GB (2011) The role of the cation aliphatic side chain length in piperidinium *bis*(trifluoromethylsulphonyl)imide ionic liquids. Electrochim Acta 57:153–159. https://doi.org/10.1016/j.electacta.2011.03.089

67. Wang M, Shan Z, Tian J, Yang K, Liu X, Liu H, Zhu K (2013) Mixtures of unsaturated imidazolium based ionic liquid and organic carbonate as electrolyte for Li-ion batteries. Electrochim Acta 95:301–307. https://doi.org/10.1016/j.electacta.2013.02.032

68. Seki S, Kobayashi Y, Miyashiro H, Ohno Y, Mita Y, Terada N (2008) Compatibility of *N*-methyl-*N*-propylpyrrolidinium cation room-temperature ionic liquid electrolytes and graphite electrodes. J Phys Chem C 112:16708–16713. https://doi.org/10.1021/jp805403e

69. Caillon-Caravanier M, Bosser G, Claude-Montigny B, Lemordant D (2002) Intermolecular interactions in lactone-based electrolytes. J Electrochem Soc 149:E340–E347. https://doi.org/10.1149/1.1499967

70. Walden P (1906) Über organische lösungs und ionisierungsmittel. III. Teil: Innere reibung und deren Zusammenhang mit dem Leitvermögen. Z Phys Chem 55:207–246. https://doi.org/10.1002/zaac.19211150103

71. Xu W, Cooper EI, Angell CA (2003) Ionic liquids: ion mobilities, glass temperatures and fragilities. J Phys Chem B 107:6170–6178. https://doi.org/10.1021/jp0275894

72. Dagoussseta L, Nguyen GTM, Vidal F, Galindo C, Auber P-H (2015) Ionic liquids and γ-butyrolactone mixtures as electrolytes for supercapacitors operating over extended temperature ranges. RSC Adv 5:13095–13101. https://doi.org/10.1039/C4RA13933J

73. Thawarkar S, Khupse ND, Kumar A (2016) Comparative investigation of the ionicity of aprotic and protic ionic liquids in molecular

solvents by using conductometry and NMR spectroscopy. PhysChemPhys 17:1006–1017. https://doi.org/10.1002/cphc.201501156

74. Canongia Lopes JN, Costa Gomes MF, Husson P, Padua AAH, Rebelo LPN, Sarraute S, Tariq M (2011) Polarity, viscosity, and ionic conductivity of liquid mixtures containing [C₄C₁im][Ntf₂] and a molecular component. J Phys Chem B 115:6088–6099. https://doi.org/10.1021/jp2012254

75. Ueno K, Tokuda H, Watanabe M (2010) Ionicity in ionic liquids: correlation with ionic structure and physicochemical properties. Phys Chem Chem Phys 12:1649–1658. https://doi.org/10.1039/B921462N

76. MacFarlane DR, Forsyth M, Izgorodina EI, Abbott AP, Annat G, Fraser K (2009) On the concept of ionicity in ionic liquids. Phys Chem Chem Phys 11:4962–4967. https://doi.org/10.1039/B900201D

77. O'Mahony AM, Silvester DS, Aldous L, Hardacre C, Compton RG (2008) Effect of water on the electrochemical window and potential limits of room-temperature ionic liquids. J Chem Eng Data 53:2884–2891. https://doi.org/10.1021/je800678e

78. Wagemaker M, Kearley GJ, van Well AA, Mutka H, Mulder FM (2003) Multiple Li positions inside oxygen octahedra in lithiated TiO₂ anatase. J Am Chem Soc 125:840–848. https://doi.org/10.1021/ja028165q

79. Fang D, Huang K, Liu S, Li Z (2008) Electrochemical properties of ordered TiO₂ nanotube loaded with Ag nano-particles for lithium anode material. J Alloys Compd 464:L5–L9. https://doi.org/10.1016/j.jallcom.2007.09.141

80. Bratić M, Jugović D, Mitrić M, Cvjetićanin N (2017) Insertion of lithium ion in anatase TiO₂ nanotube arrays of different morphology. J Alloys Compd 712:90–96. https://doi.org/10.1016/j.jallcom.2017.04.065

81. Jiang C, Wei M, Qi Z, Kudo T, Honma I, Zhou H (2007) Particle size dependence of the lithium storage capability and high rate performance of nanocrystalline anatase TiO₂ electrode. J Power Sources 166:239–243. https://doi.org/10.1016/j.jpowsour.2007.01.004

82. Gupta H, Kataria S, Balo L, Singh VK, Kumar Singh S, Tripathi AK, Verma YL, Singh RK (2018) Electrochemical study of ionic liquid based polymer electrolyte with graphene oxide coated LiFePO₄ cathode for Li battery. Solid State Ionics 320:186–192. https://doi.org/10.1016/j.ssi.2018.03.008

83. Singh SK, Gupta H, Balo L, Shalu SVK, Tripathi AK, Verma YL, Singh RK (2018) Electrochemical characterization of ionic liquid based gel polymer electrolyte for lithium battery application. Ionics 24:1895–1906. https://doi.org/10.1007/s11581-018-2458-x